A Study of High-Speed Aerodynamic Configurations for Increased Lateral-Directional Controllability

Connor S. Hoopes, [1]
and
Timothy T. Takahashi[2]
Arizona State University, Tempe, AZ 85287

This paper investigates the configurations needed to demonstrate positive lateral-directional controllability across the flight envelope of a hypersonic vehicle. We examined the NASA Space Shuttle Orbiter as a baseline reference configuration. The Orbiter had limited high-speed maneuvering capability; it relied on reaction-control jets to augment controllability due to a strong tendency for its aerodynamics to "control couple." We realize that many problems associated with the control of the hypersonic Orbiter are due to its slender configuration. This work relies upon the Evolved-Bihrle-Weissman chart as an accurate indicator of lateral-directional stability and controllability to explore variant configurations to shown how large wing tip fins may reduce its dependence on reaction control.

I. Introduction

The development of a truly general purpose, air-breathing maneuvering hypersonic flight vehicle has largely eluded the aerospace community. On one hand we have recent limited maneuverability air-breathing hypersonic propulsion testbeds like the NASA Hyper-X [1] and Air Force X-51 [2] on the other hand, we have the broadly maneuvering integral-rocket propelled NASA/Air Force/North American X-15 [3] from the 1960's. Also in the mix is the NASA/Rockwell Space Shuttle orbiter, which is "flown" as a glider during reentry with significant down-range and cross-range maneuvering performance. Little publicly released data exists detailing the aerodynamic stability of Hyper-X and X-51while considerable detailed data exists for both the X-15 and the Orbiter. [4][5]

The Space Shuttle Orbiter successfully flew many missions spanning both the hypersonic, supersonic and the subsonic flight regimes; the Shuttle orbiter reached speeds in excess of Mach 25 on reentry. The "hypersonic" regime unequivocally encompasses operations above Mach 5; but the distinction between supersonics and hypersonics is not always clear. Above Mach 3 and below Mach 8, where air dissociates into a plasma, exists a region where classical design principles like "simple sweep theory" and "slender body theory" no longer apply but flow remains amenable to be analyzed using linear potential flow codes. Above these speeds, "real gas effects" became significant as the flow around the Orbiter would partially dissociate, enveloping it in plasma. [7] The flight conditions and flight dynamics problems discussed in the paper will be restricted to flight conditions where "real gas effects" are not significant.

Since the Orbiter operated over a wide range of speeds, we must understand how its respective aerodynamic properties varied across its flight envelope. [7] As the freestream Mach numbers increase from subsonic to hypersonic, the source of lift changes from being leeward surface dominated (upper surface "suction side") to windward surface dominated (lower surface "impact pressure side"). This results in strong changes in fundamental vehicle level aerodynamic properties at increased Mach numbers; see FIGURE 1.

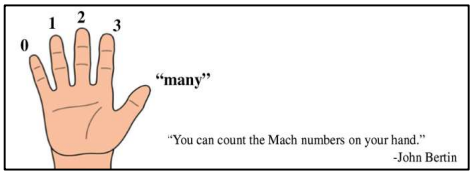

FIGURE 1. Hypersonic Flight Issues [7]

[1] M.S. Candidate – Aerospace Engineering, School for the Engineering of Matter, Transport and Energy, Arizona State University, Tempe, AZ. AIAA Student Member.
[2] Professor of Practice – Aerospace Engineering, School for the Engineering of Matter, Transport and Energy, Arizona State University, Tempe, AZ. AIAA Associate Fellow.

A general-purpose flight vehicle must demonstrate positive stability and controllability over a range of speeds, altitudes, and weights. From a flight control perspective, positive stability means a tendency to respond to disturbances through damped oscillations about a baseline state. A vehicle may attain positive stability by 1) inherent aerodynamic static stability or 2) through some form of active closed-loop control or 3) through a combination of both. Controllability means that the pilot, or autopilot, can direct changes in vehicle speed, altitude, and heading which the vehicle will follow. Satisfactory controllability requires both sufficient authority, (the ability to generate forces and moments) and frequency bandwidth (the ability for the vehicle to follow a close succession of differing commands).

Since hypersonic vehicles, such as the Orbiter, tend to be long and slender, they have mass properties that accentuate lateral-directional cross-coupling. [8] As flight speeds increase, the windward surface dominated aerodynamics degrade inherent static directional stability. High Mach numbers also reduce all forms available aerodynamic control power. Taken together, the configurator of the aerodynamic shape of a hypersonic vehicle must carefully consider the implication of the proposed loft on the "quantity" and "quality" of the basic aerodynamic stability, terms like $dCm/d\alpha$, $dCn/d\beta$, and $dCl/d\beta$. The "quantity" of aerodynamic control power are terms like *dCm/delevator*, *dCn/drudder,* or *dCl/daileron*. The "quality" of aerodynamic control power is the magnitude of un-intended byproducts of control surface movement, things like static directional stability changes due to elevator deflection, or adverse-yaw-due-to-roll from the ailerons, or even adverse-roll-due-to-yaw from the rudder.

Recent work at Arizona State University (ASU), often in collaboration with the Air Force Institute of Technology (AFIT), [9][10][11][12] has highlighted how important aerodynamic control-coupling metrics developed to support transonic maneuvering fighter aircraft are to screen candidate hypersonic and other high-speed configurations. For lateral-directional stability "quantity" and control "quality," a diagram known as the Bihrle-Weissman Chart proves to be an effective indicator of hypersonic flying qualities; see FIGURE 2.[13] For example, the USAF/NASA/North American X-15 proved to have inherently favorable flying characteristics according to Bihrle-Weissman criteria; and indeed, pilots flew over two hundred successful missions. Provided the X-15 was flown within the atmosphere (i.e., at reasonable dynamic pressure) its inherent aerodynamic stability and controllability was sufficient for controlled maneuvering flight. Only when flown at the outer reaches of the atmosphere, at low dynamic pressure, did it require reaction-jet thrusters to command attitude.

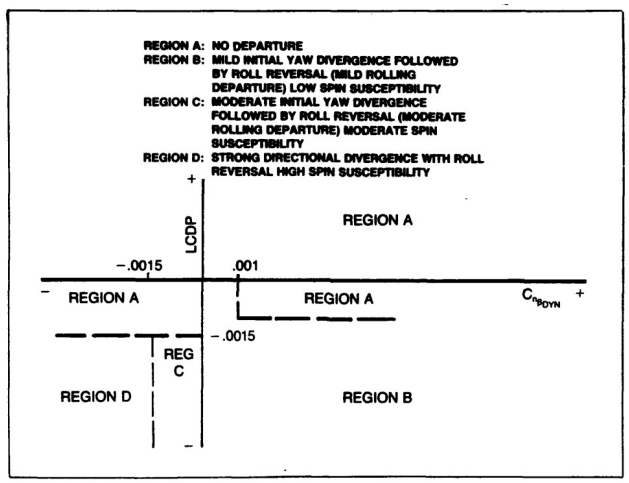

FIGURE 2. Weissman Chart [14]

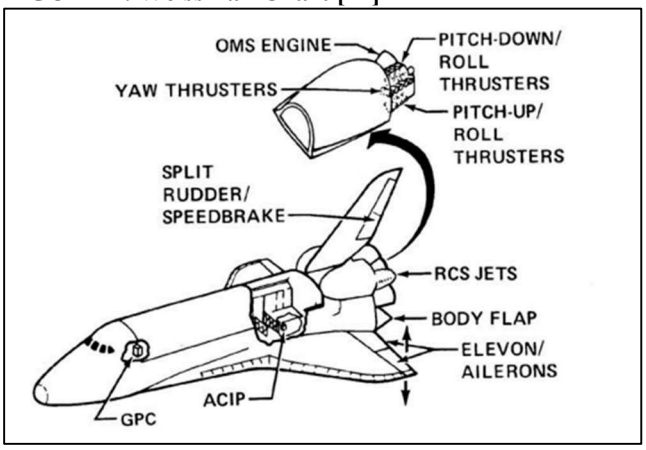

FIGURE 3. Shuttle configuration [17]

Conversely, the ASU/AFIT team noted that the Shuttle Orbiter needed to use its reaction control system (RCS) thrusters deep into atmosphere at speeds as low as Mach 1, mere minutes before touchdown; see FIGURE 3. A NASA flight test report noted that "stability augmentation is provided by the aft reaction control system (RCS) jets… The aft yaw jets are active until Mach 1, while the pitch and roll jets are terminated at a pressure of 20 and 10 pounds per square foot, respectively." [15] Thus, we realized that a configuration like the X-15 has nearly unlimited hypersonic maneuvering capability while the Shuttle Orbiter's atmospheric maneuvering capability is limited by the propellant load feeding and size of the thrusters of its RCS system. [16] Since the Shuttle was never flown on polar orbit missions, which would require substantial hypersonic maneuvering, suggests that the need for

active RCS augmentation at all supersonic speeds substantially limited its endo-atmospheric hypersonic performance; the Orbiter probably never could achieve the necessary cross-range to reliably fly from Vandenberg.

In this work, we will consider the Shuttle Orbiter baseline and consider what aerodynamic modifications would be necessary in order for it to dispense with its RCS during atmospheric reentry and gliding flight at reasonable dynamic pressures.

II. What is a Weissman Chart?

Aircraft designers seek rapid methods to screen candidate configurations for inherently favorable or unfavorable flying qualities. The "Weissman Chart" proves to be a durable metric; it was proposed in 1972 by Robert Weissman in an M.S. Thesis at the University of Dayton; return to FIGURE 2. [14] "Weissman developed this criterion from analyzing time history sensitivity studies to lateral/directional static stability derivatives in a digital six degree-of-freedom off-line simulation. Based on time history traces, Weissman empirically identified regions of increasing roll departure severity and spin susceptibility." [18]

The two axis that are used in the chart represent $Cn_{\beta DYN}$ and $LCDP$. $Cn_{\beta DYN}$ is the Dutch-Roll Stability parameter (yawing moment coefficient with respect to side slip adjusted for vehicle mass properties) and the $LCDP$ is the Lateral Control Departure Parameter, a metric of the "quality" of the aileron effect of the lateral control surfaces. [14][19][20][21]

$$Cn_{\beta DYN} = \frac{dCn}{d\beta} * cos(\alpha) - \frac{dCl}{d\,\beta}\left(\frac{I_{zz}}{I_{xx}}\right) * sin(\alpha) \quad (1)$$

$$LCDP = \frac{dCn}{d\beta} - \frac{dCl}{d\beta} * \frac{\frac{dCn}{d\,aileron}}{\frac{dCl}{d\,aileron}} \quad (2)$$

In a companion paper to be published at the 2023 AIAA Aviation Conference, Takahashi, Griffin & Grandhi present an evolved version of this chart; refer to FIGURE 4. [22] Their work builds on earlier efforts by Bihrle, Weissman and Mason [13] among others. Their revision addresses the challenges of slender, high-speed vehicles first noted by Skow [23] with the Northrop T-38/F-5 and their own review of observed flying qualities deficiencies of the Bell X-2. They moved the boundary of the "F" to "A" region to require additional open loop Dutch Roll stability to guarantee "Highly Departure and Spin Resistant Flight." Ideally, a general-purpose maneuvering vehicle will need to have its "open-loop" aerodynamics firmly planted in region "A" of the Evolved-Bihrle-Weissman Chart.

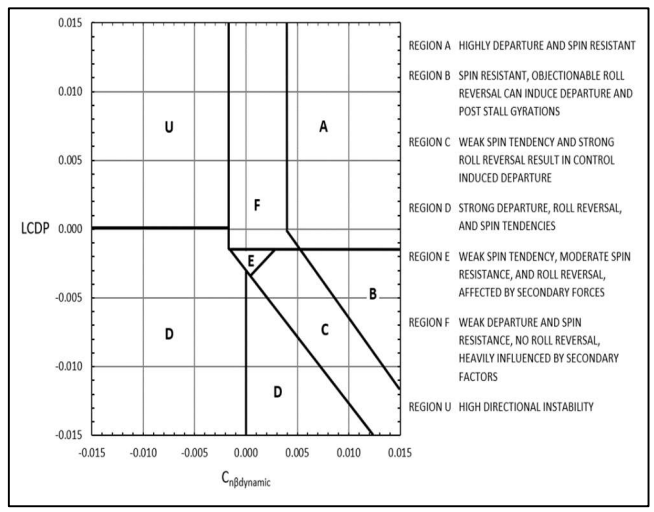

FIGURE 4. Evolved Bihrle-Weissman Chart after Takahashi, Griffin & Grandhi [22]

Aircraft have no inherent desire to stay right-side up as their aerodynamics are usually capable of overwhelming whatever "pendulum stability" they may possess. Thus, to maintain nominally "straight-and-level" flight, aircraft must be locked into a stable oscillatory "Dutch-Roll" mode where they gently rock back and forth in a combined rolling and yawing motion. [20][24][25][26]

Directional stability must be maintained for an aircraft to be stable in forward flight; otherwise, it will diverge in course heading. Since aircraft must weathercock into the wind, rather than depart, they must display $dCn/d\beta > 0$ whether by inherent aerodynamic effects or through closed loop control. Typical low speed aircraft have large tails and develop weathercock stability entirely through passive aerodynamic effects. Other vehicles, such as rockets or stealth aircraft, may utilize a closed-loop feedback control system using either active rudder control, active laterally disposed drag brake control and/or vectored thrust to develop their synthetic stability. We will see here that the Space Shuttle Orbiter lacked sufficient inherent aerodynamic stability; it relied upon reaction control jets (RCS) to keep its nose pointed forwards. [12][16]

Aerodynamic lateral stability is commonly associated with the effects of positive effective dihedral. Thus, to be stable laterally, the aircraft must develop a rolling moment to oppose sideslip: $dCl/d\beta < 0$ whether by inherent aerodynamic effects or through closed loop control.

All factors taken together, the aircraft designer must be vigilant so that the proposed vehicle is **not** directionally divergent, never expresses unstable Dutch Roll, does not exhibit Control Coupling that leads to an inadvertent spin, and avoids negative damping associated with Inertial Coupling. [20][21]

The Dutch Roll mode is the easiest to assess. Recall that it is a combined lateral-directional motion. [20] At first order, we may estimate it by:

$$\omega_{dr} = \frac{1}{2\pi}\sqrt{\frac{57.3 * Cn_{\beta DYN} * q * S_{ref} * b}{Izz}} \qquad (3)$$

Thus, an oscillatory Dutch Roll Frequency exists proportional to the square root of $Cn_{\beta DYN}$, provided that, it is positive. The frequency also scales proportional to the square root of the dynamic pressure and inversely proportional to the square root of the mass-moment-of-inertia in yaw. MIL-STD 8785C [27] and MIL-STD 1797A [28] provide guidelines to the preferred frequency range for the Dutch Roll. MIL-STD 8785C recommends minimum Dutch Roll Frequencies for design; it should not be so slow to lead to phase-lag when the pilot (or autopilot) commands maneuvers. While MIL-8785C has no upper bound, it should not be so fast as to provoke structural resonance. [20] However, as the frequency increases, the aircraft will become more responsive to roll inputs.

If $Cn_{\beta DYN}$ is negative, the Dutch Roll frequency becomes an imaginary number, i.e., it is divergent and indicates an inherent tendency for the vehicle to go out of control. There are several ways $Cn_{\beta DYN}$ can be negative; the Dutch Roll mode can be unstable where despite positive static directional stability, the aircraft experiences overall lateral-directional instability; this is when $dCl/d\beta > 0$ and overwhelms the stabilizing contributions of $dCn/d\beta > 0$. On the flip side, an aircraft that lacks static directional stability can have overall lateral-directional stability provided it has enough effective dihedral; this exists only when $dCl/d\beta << 0$. Since static directional stability ($dCn/d\beta$) declines with increasing Mach number, many designers of high-speed vehicles (including those who configured the Space Shuttle Orbiter) exploit the very strong effective dihedral of a highly swept wing flown at high angles of attack to get positive $\mathrm{Cn}_{\beta\mathrm{DYN}}$ despite poor static directional stability.

The Space Shuttle Orbiter conceptual designers may have overlooked the magnitude of the problem associated with Control Coupling while prioritizing other features. This is the factor associated with *LCDP*. Control Coupling occurs when static yaw and roll stability interact with the moments from control surfaces in a manner that is destabilizing. Pilots can no longer trim their aircraft in yaw and roll. They also describe situations where the 'controls reverse'.

Since $LCDP = \frac{dCn}{d\beta} - \frac{dCl}{d\beta} * \frac{\frac{dCn}{d\,aileron}}{\frac{dCl}{d\,aileron}}$ and needs to be positive, a vehicle needs to have sufficient stick-fixed directional stability ($dCn/d\beta > 0$) to balance the remainder of the right-hand-side of the equation. Because $dCl/d\beta < 0$ for slender swept-configurations at positive-angle-of-attack, the sign of the yaw-to-roll-ratio of the "aileron" controls is critical determining whether *LCDP* is positive or negative. A slender, swept vehicle with unfavorable "adverse yaw" from its "ailerons" tends to negative *LCDP*. When an aircraft has adverse aileron control where, in the absence of pilot applying opposing rudder, roll command inputs will destabilize the aircraft in yaw.

LCDP, as applied to the Bihrle-Weissman chart, may represent either the simple "open-loop" or the "closed-loop" performance of the "ailerons." On a typical aircraft, designers implement "Aileron-Rudder-Interconnect" to automatically apply some rudder in conjunction with aileron to reduce (or eliminate) adverse yaw. If adverse yaw were to be eliminated, $LCDP \approx \frac{dCn}{d\beta}$; which so long as $\frac{dCn}{d\beta} > \sim +0.004$ would place the vehicle in region "A" of the Bihrle-Weissman chart. Aileron-Rudder-Interconnect is a "feed-forward" control law that reflects the "closed-loop" augmented performance of an aircraft. For the Shuttle Orbiter, the "open loop" *LCDP* represents the totality of usable aerodynamic control as *ARI* is not a viable control law; this is because the split-rudder can only rarely be used as an effective yaw control device. At

supersonic speeds the split rudders are fully open in "speed brake" mode to help augment static directional stability; at subsonic speeds they are scheduled partially open as “speed brakes” and then opened and closed as necessary to modulate drag so that the pilot can independently control speed and sink rate. Substantial classical rudder control is only usable moments before a crosswind touchdown; when the speed-brake function can be disabled. As such, the only remaining control device to counteract the adverse yaw of the ailerons (and improve *LCDP*) are the lateral reaction control system (*RCS*) hydrazine jets.

III. Basic Approach to Analyze the Space Shuttle Orbiter

Our Space Shuttle Orbiter design study considers both the baseline Orbiter, as fielded in gliding drop tests and on 135 orbital missions, and proposed variants of the Orbiter designed to have improved gliding maneuverability obviating the need for RCS control deep in the atmosphere.

For the baseline Orbiter, we plot flight-test reduced data onto the evolved Bihrle-Weissman chart. We also develop general aerodynamic databases for the baseline and proposed variant configurations.

A. FLIGHT TEST

We extracted flight test data from a number of papers published by NASA/Langley arising from a 1983 “Lessons Learned” conference. [5] We source much of our comparison data from a paper given at that conference titled “Stability and Control Over the Supersonic and Hypersonic Speed Range.” [29] This source provided the rolling moment and yawing moment charts used for the Bihrle-Weissman chart analysis and is the baseline for the comparison to the models for accuracy and model validity. We also rely on other sources for general background information regarding Shuttle Orbiter nominal re-entry trajectories as well as the final approach and landing. [6][30][31][32][33][34] With the availability of very detailed flight histories, we reconstructed the a trajectory with known control surface commands; see TABLE 1.

TABLE 1. Reconstructed Flight Data

Mach	Alpha	Elevon	BodyFlap	SplitFlap	L/D	CL	CD	CnB	ClB	Cnda	Clda
2	12	5	-4			0.4	0.2	-0.0008	-0.0015	-0.0002	0.0012
4	20	5	4	75	1.8077	0.42	0.25	-0.0017	-0.0016	-0.0003	0.0009
6	27	3.25	6	85	1.5349	0.51	0.31	-0.0018	-0.0017	-0.0004	0.00122
8	34	2.5	8	85	1.295	0.72	0.52	-0.0015	-0.0021	-0.0004	0.0015
10	39	1	8	85	1.1012	0.851	0.8	-0.0016	-0.002	-0.0005	0.00165
12	40	1	8	0	1.0745	0.9	0.9	-0.0016	-0.0021	-0.0005	0.0017
14	40	1	8	0	1.0745	0.9	0.85	-0.0016	-0.0021	-0.0005	0.00173
16	40	1	8	0	1.0745	0.9	0.85	-0.0016	-0.0021	-0.0005	0.00175
18	40	1	8	0	1.0745	0.85	0.79	-0.0016	-0.0021	-0.0006	0.00176
20	40	1	8	0	1.0745	0.85	0.79	-0.0016	-0.0021	-0.0006	0.00176
22	40	1	8	0	1.0745	0.85	0.8	-0.0016	-0.0021	-0.0006	0.00177
24	40	1	8	0	1.0745	0.85	0.76	-0.0016	-0.0021	-0.0008	0.002
26	40	1	8	0	1.0745	0.85	0.76	-0.0016	-0.0021	-0.0009	0.0021

B. VORLAX

VORLAX is a vortex lattice potential flow solving panel-method Computational Fluid Dynamics (CFD) code written in FORTRAN. [35][38] It can be used to determine lift, inviscid drag, and the stability derivatives of arbitrary configurations. It has both subsonic and supersonic leading edge flow models. The supersonic leading-edge flow model accounts for shock waves developed at the leading and trailing edges; as such, it is valid for “slender” shapes that do not develop off-body standing shock waves. VORLAX solutions fundamentally neglect thickness effects, and as such will under-predict the directional stabilizing effect of the Orbiter’s split-wedge “speed brake” rudder. It also cannot capture any sort of “real-gas-effects” of high temperature air. Despite these limitations, Griffin & Takahashi showed that it worked remarkably well to estimate the aerodynamic stability of the X-15 up through Mach 6. [12]

IV. Baseline Orbiter Lateral-Directional Control Issues Seen in Flight Test

In this section, we will use flight test aerodynamic data to estimate the lateral-directional stability of the Orbiter, assess it with the Evolved-Bihrle-Weissman criteria and compare against flight test experience.

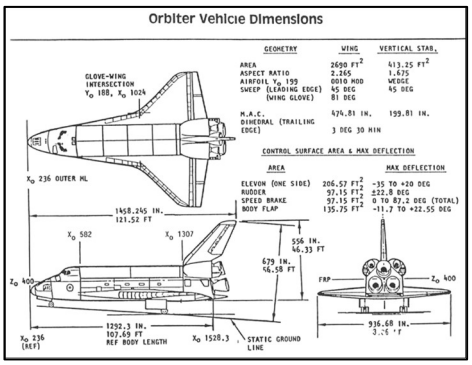

FIGURE 5. Orbiter Shuttle Dimensions [38

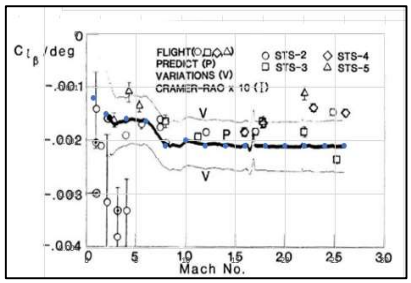

FIGURE 6. Shuttle Flight Test $dC_l/d\beta$[29]

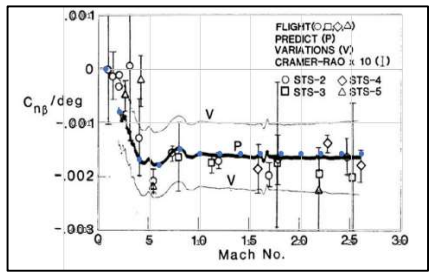

FIGURE 7. $dC_n/d\beta$[29]

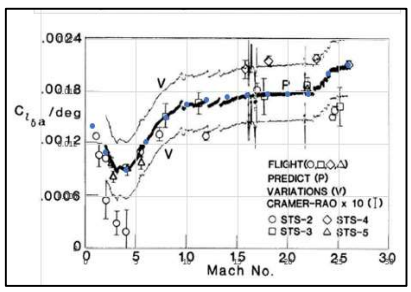

FIGURE 8. $dC_l/dail$[29]

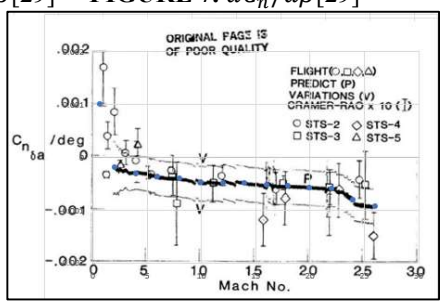

FIGURE 9. $dC_n/dail$[29]

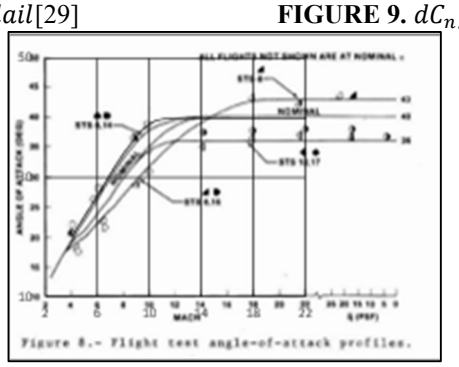

FIGURE 10. Mach Number vs Angle of Attack [17]

The aerodynamic database understands the response of the Orbiter due to changes in Mach number, angle-of-attack (α), sideslip (β), or control surface deflection. We compute basic, longitudinal aerodynamics at zero sideslip (β=0°) as a function of the angle-of-attack (α): specifically pitching moments (C_m) and the lift coefficient (C_L). For the lateral-directional screening, we compute the small sideslip linearized derivatives of yawing moment due to sideslip (dC_n / $d\beta$) versus angle-of-attack (α) and rolling moment due to sideslip (dC_l / $d\beta$) versus angle-of-attack (α). Reference dimensions may be seen in FIGURE 5.

In order to find the baseline *LCDP* and $Cn_{\beta DYN}$ values four key values were necessary, those being Cl_β, $C_{n\beta}$, C_{lda}, and C_{nda}. Through the equations (1) and (2), the results can be plotted on the Evolved-Bihrle-Weissman Chart (recall FIGURE 4).

The flight data that was utilized can be seen FIGURES 6 through 9. They provided the Cl_β, $C_{n\beta}$, $C_{l\gamma a}$, and $C_{n\gamma a}$ all per deg and through the shuttles entire flight regime; shuttle reports present the data in BODY AXIS. That being the hypersonic region all the way down to subsonic region. In order to back out the necessary values from the "per deg" values present in the charts to the values needed for the *LCDP* calculations, specific Mach numbers would need to be selected and that control point's corresponding Angle-of-attack could be used. See FIGURE 10 for the angle-of-attack schedule. [17]

The $Cn_{\beta DYN}$ is reliant on the ratio of the Mass Moments of Inertia. For the calculations we take the value for the *Izz/Ixx* = 8.01 as given for STS-1. [29] [34]

With the angle-of-attack schedule (FIGURE 10), and the yaw-rolling moment charts (FIGUREs 6 thru 9), we calculated *LCDP* and $Cn_{\beta DYN}$. We show tabulated values for the given control points in Table 2, below.

The Evolved-Bihrle-Weissman Chart for the baseline shuttle could then be presented from the tabulated values from the flight test data; see FIGURE 11.

Examining FIGURE 12, the Evolved-Bihrle-Weissman Chart for the Space Shuttle Orbiter, we see the following trends on re-entry:

1. At the highest Mach numbers, early during re-entry where dynamic pressure is low and the Orbiter is flown far nose-up, its performance straddles the line between the stable region "A" and the unstable regions "B" and "C." While $Cn_{\beta DYN}$ is strongly positive, *LCDP* is nearly zero; clearly closed-loop RCS control is needed here.
2. As we decelerate down to Mach 6, at *ALT*=150,000-ft at with dynamic pressure of 100-psf and attain 171-KEAS, as seen in FIGUREs 12 and 13, around the 1,600 second mark, we are now in a region where aerodynamic

TABLE 2. Table of values and calculations for $LCDP$ and $Cn_{\beta DYN}$

Mach	0.7	2	4	6	8	10	12	14	16	18	20	22	24	26
Alpha	4	12	20	30	37	39	40	40	40	40	40	40	40	40
CnB	0	-0.0008	-0.0017	-0.0018	-0.0015	-0.0016	-0.0016	-0.0016	-0.0016	-0.0016	-0.0016	-0.0016	-0.0016	-0.0016
ClB	-0.0012	-0.0015	-0.0016	-0.00165	-0.0021	-0.002	-0.0021	-0.0021	-0.0021	-0.0021	-0.0021	-0.0021	-0.0021	-0.0021
Cnda	0.001	-0.0002	-0.00031	-0.00036	-0.0004	-0.00047	-0.0005	-0.0005	-0.00052	-0.00055	-0.00058	-0.0006	-0.0008	-0.00094
Clda	0.014	0.011	0.009	0.0122	0.015	0.0165	0.017	0.0173	0.0175	0.0176	0.0176	0.0177	0.02	0.021
IZZ/IXX	8.04	8.04	8.04	8.04	8.04	8.04	8.04	8.04	8.04	8.04	8.04	8.04	8.04	8.04
Calculations														
CnBdynamic	0.00067	0.00172	0.00280	0.00507	0.00896	0.00888	0.00963	0.00963	0.00963	0.00963	0.00963	0.00963	0.00963	0.00963
LCDP	0.00009	-0.00083	-0.00176	-0.00185	-0.00156	-0.00166	-0.00166	-0.00166	-0.00166	-0.00167	-0.00167	-0.00167	-0.00168	-0.00169

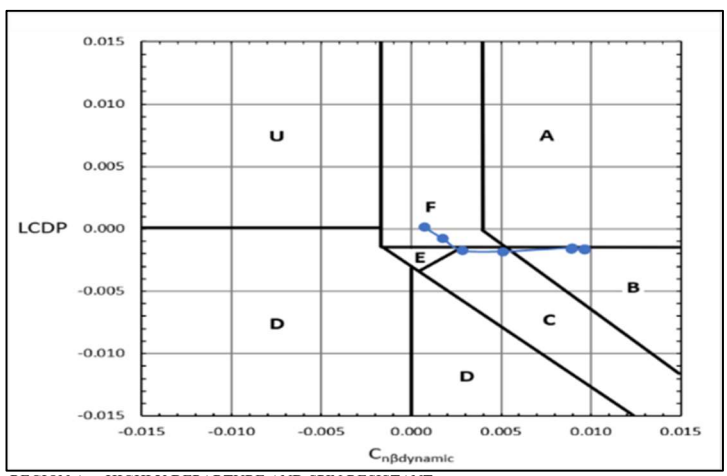

REGION A HIGHLY DEPARTURE AND SPIN RESISTANT
REGION B SPIN RESISTANT, OBJECTIONABLE ROLL REVERSAL CAN INDUCE DEPARTURE AND POST STALL GYRATIONS
REGION C WEAK SPIN TENDENCY AND STRONG ROLL REVERSAL RESULT IN CONTROL INDUCED DEPARTURE
REGION D STRONG DEPARTURE, ROLL REVERSAL, AND SPIN TENDENCIES
REGION E WEAK SPIN TENDENCY, MODERATE SPIN RESISTANCE, AND ROLL REVERSAL, AFFECTED BY SECONDARY FORCES
REGION F WEAK DEPARTURE AND SPIN RESISTANCE, NO ROLL REVERSAL, HEAVILY INFLUENCED BY SECONDARY FACTORS
REGION U HIGH DIRECTIONAL INSTABILITY

FIGURE 11. Evolved-Bihrle-Weissman Chart based on Shuttle Flight Test

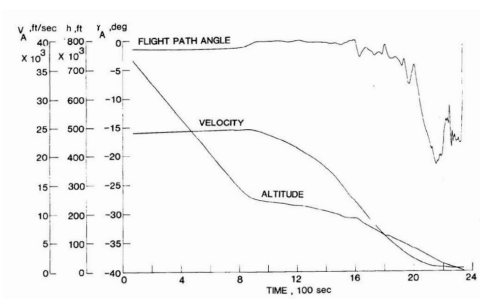

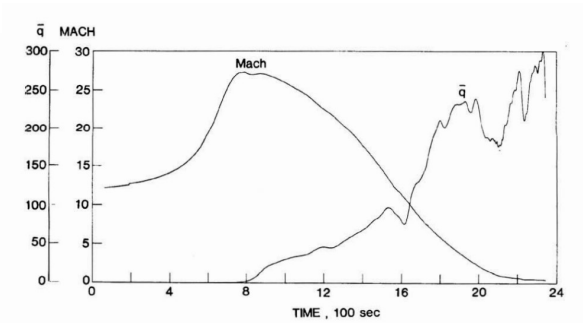

FIGURE 12. Dynamic Pressure vs. Time [29] **FIGURE 13. Mach Number vs. Time [29]**

control "*should"* reasonable. However, the shuttle aerodynamics continue to have poor *LCDP*; thus, absent RCS control power augmentation it has weak spin tendencies and will exhibit un-intentional roll-reversals.

3. As the shuttle further decelerates and sinks deeper into the atmosphere to Mach 4, about the 1,700 second mark at an altitude of 90,000-ft and approximate dynamic pressure equaling 150-psf and attains ~245-KEAS, the shuttle is now in a region "C" where strong roll reversals are likely to result in control induced departure.
4. At Mach 2, around the 1,900 seconds with a dynamic pressure of 170-psf, at an altitude of 65,000-ft and the nose is lowered to α=~12°. We are now approaching the terminal area at ~225-KEAS. We are now in a region "F" with weak departure and spin resistance where controllability is heavily influenced by secondary factors.
5. On subsonic final gliding approach, where α=~4° we remain firmly in region "F" with weak departure and spin resistance where controllability is heavily influenced by secondary factors. $Cn_{\beta DYN}$ is now quite small, once again highlighting the relatively weak static directional stability of the Orbiter (despite its visually imposing, large – but short coupled – vertical fin.)

Our interpretation of Bihrle Weissman criteria closely matches NASA flight operations results.

In reality, the shuttle relied on its RCS thrusters in order to remain stable and controllable from initial reentry down to Mach 1.2. [32] In another report, NASA specifically stated that "analysis indicated that the problem was caused by a sign change in the *LCDP* in the Mach 5 region. As a partial result of this problem, several changes were made to the (flight control system). The basic FCS design was changed from the aileron bank control to a system utilizing the yaw RCS jets to initiate bank maneuver and the ailerons to coordinate the maneuvers prior to activation of the rudder. After the rudder became active, a gradual FCS gain change produced the conventional aileron bank control with rudder coordination…. The orbiter FCS utilizes a side acceleration feedback to the rudder and yaw jets to provide stability augmentation." [37]

NASA further stated that, "Very little improvement is shown for the rudder augmentation. This is due to the small rudder effectiveness which results from the aeroelasticity effects and from application of aerodynamic variations. It is evident that the RCS provides a significant improvement…At the first bank maneuver which occurred very early in the entry, a large sideslip oscillation developed with β reaching a value of 3.5°. Post flight analysis showed the primary culprit to be the rolling moment RCS jet interaction." [32]

V. Computational Study of Baseline Orbiter Aerodynamics

A. Subsonic and Supersonic Flight Regime

The supersonic/subsonic model was made in VORLAX; see FIGURE 14. The geometry derives from NASA published dimensions [40] shown previously as FIGURE 5, above. This model was meant to capture key features such as leading-edge sweep along the wing and wing glove, wingspan, and the overall body dimensions. A feature that could not be captured in the model was the split rudder / drag brakes on the vertical stabilizer. The combination of overlapping panels would not bode well for VORLAX.

Our VORLAX model had S_{re} =2690 ft^2, reference chord $\bar{c}$ =39.6-ft, and wingspan b=78.1-ft. These all match the NASA dimensions.[38] The center of gravity for the model has a CG location of $\bar{x}$ of 71.40 ft and $\bar{z}$ of 12.5 ft. [38][39]

FIGUREs 15 and 16 (overleaf) compares basic aerodynamic parameters such as $C_{l_\beta}, C_{n_\beta}, C_{Y_\beta}, C_N, and\ C_m$ between VORLAX and the "official" Orbiter database. We see that there is relatively close agreement between the VORLAX model and the subsonic wind tunnel and flight data; most of the time the VORLAX results are within the official "uncertainty band." The panel method continues to match in accuracy to both the normal force C_N and pitching moment C_m. The one exception is static directional stability, Cn_β; this is due to the rudder effectiveness with the split flap. The split rudder was deployed as a drag brake in both flight test and wind tunnel tests; it cannot be modeled using the panel code.

We see that for the shuttle at sideslip, the vehicle remains stable through all angles of attack. The positive nature of C_{n_β} helps to maintain yaw stability. The general negative behavior and decline in C_{l_β} represents an effective increase "Dihedral Effect" which leads to an overall stable rolling moment. The constant value and negative magnitude of the side force C_{Y_β} at slide slip further indicate the stability of the vehicle.

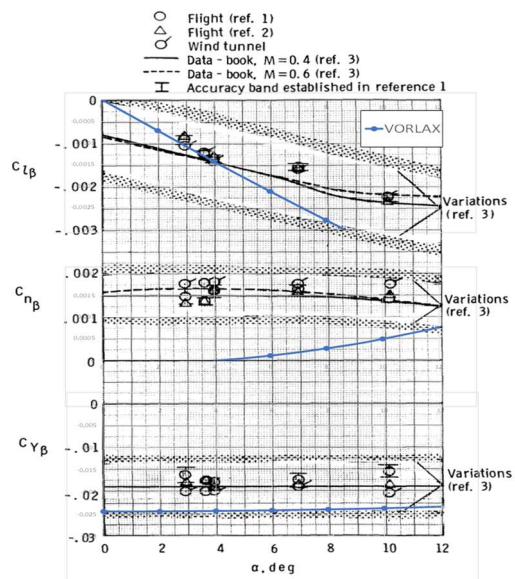

FIGURE 15. Subsonic Flight Data comparison to VORLAX $C_{l_\beta}, C_{n_\beta}, C_{Y_\beta}$ [39].

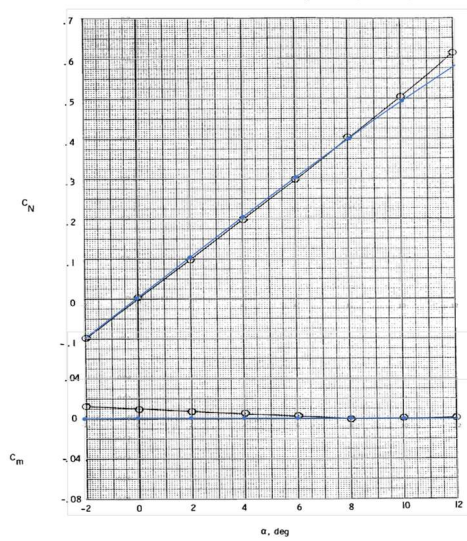

FIGURE 16. Subsonic Flight Data comparison to VORLAX C_N & C_m [39].

It is key to note that C_{n_β} is relatively close to zero. This indicates that the lateral-directional stability is fragile and could be destabilized depending on flight trajectory and commands. In fact, the VORLAX model, which does not include the split flap, has a negative region that is unstable. The NASA report for the correlation of the wind tunnel data and flight test results from which the figures are pulled have only tests conducted split flap open configurations. This would seem as though the split flap feature may be necessary for stability and very fragile. This is evident in a NASA report [40], when they state, "Component buildup studies showed that the vertical tail contributed to the measured lateral and directional instabilities at the lower Reynolds numbers and angles of attack."

In the buildup study performed NASA [40] they concluded that the "component buildup studies showed that the vertical tail contributed to the measured lateral and directional instabilities at the lower Reynolds numbers and angles of attack…The most significant change in lateral stability incurred by removal of a configuration component[s]…The removal of the OMS pods in this case reduces the stability level…and the stability level is shown to increase slightly with the removal of the vertical tail" This illustrates the fragile nature of the lateral directional stability and its dependencies on the configuration. Furthermore, we see that for the results of the computational study as they relate to the accuracy of the model, that the inability to model the split flap and the OMS pods would explain the differences in C_{l_β} but would otherwise be accurate.

With the computational model showing to be relatively accurate, we can make further comparisons to verify the performance of the model at higher Mach numbers.

B. Hypersonic Flight Regime

The model was further run for Mach 0 to 30 and compared against known flight test data [31]. The results show the relative accuracy of VORLAX into the hypersonic regime.

We see that the for the side force coefficient at sideslip, C_{Y_β} in FIGURE 17 matches close to the overall trend and magnitudes of the flight test data. The pitching moment, C_{m_α}, matches relatively well as seen in FIGURE 18.

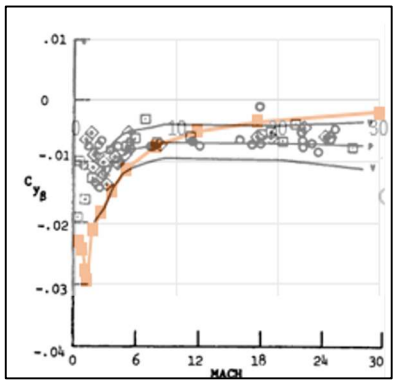

FIGURE 17. Hypersonic Comparison to VORLAX C_{Y_β}[31].

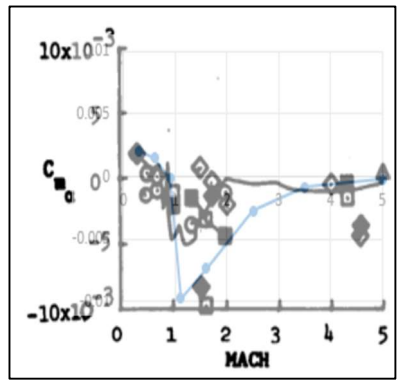

FIGURE 18. Hypersonic Comparison to VORLAX C_{m_α}[31].

For C_{n_β} and C_{l_β}, seen in FIGURE 19 and FIGURE 20 respectively, the VORLAX results vary from the flight test results. For C_{n_β} in FIGURE 19, although the VORLAX results do not match in magnitudes to the flight test results, they do match in trend. They both rise and sharply decline below MACH 6 and then plateau till the top of the flight regime. This would validate the VORLAX ability to predict trends while the results may vary in scale. This however not true for C_{l_β} in FIGURE 20. We see that the trend nor the magnitudes of the VORLAX results do not match the flight test results. This inconsistency is okay as it is explainable with the subsonic VORLAX model and the results of the subsonic wind tunnel test.

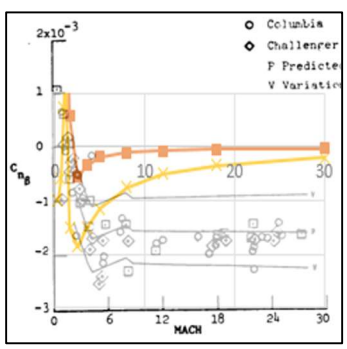

FIGURE 19. Hypersonic Comparison to VORLAX C_{n_β}[31].

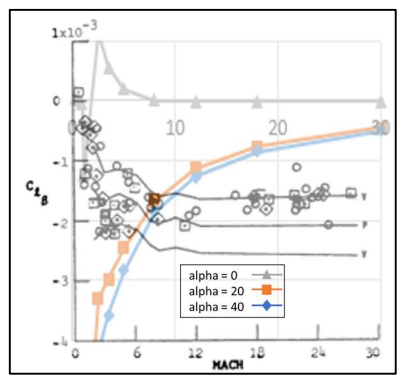

FIGURE 20. Hypersonic Comparison to VORLAX C_{l_β}[31].

Hypersonic flight involves real gas and viscous effects both of which are not within the capability of the inviscid methods of VORLAX. The accuracy of the results are predicated upon the validation to the flight test and wind tunnel results. We showed that the VORLAX results are accurate in trend and magnitude to the flight data. In addition to the relatively small values of the yaw, pitch, and roll coefficients that exist in the hypersonic regime, the VORLAX results do not misrepresent those values either. Therefore, we constrained our results to Mach 6, to ensure that the results stay true to the flight test results and ensure that, notwithstanding VORLAX's lack of capability to model real gas and viscous forces, the results can still be valid in this specific case.

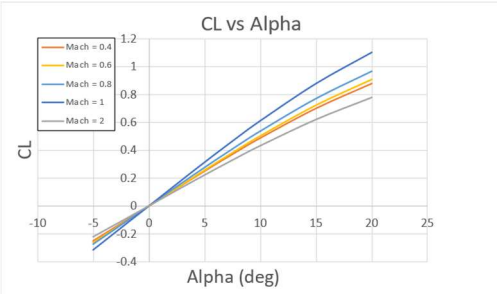

FIGURE 21. Baseline Shuttle C_L vs α

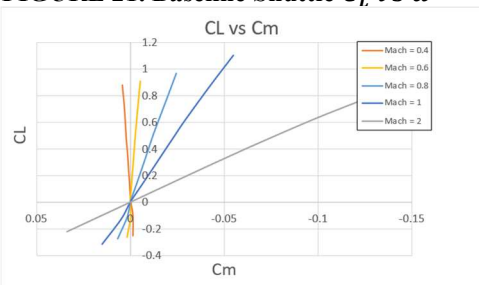

FIGURE 22. Baseline Shuttle C_L vs C_m

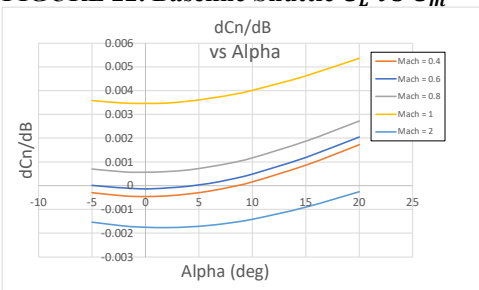

FIGURE 23. $dC_n/d\beta$ vs α

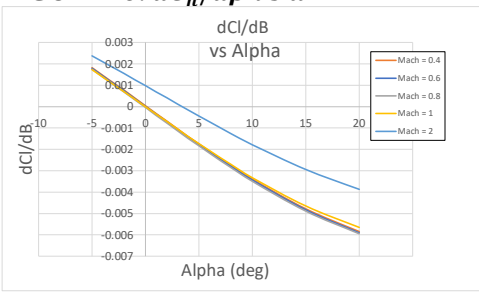

FIGURE 24. $dC_l/d\beta$ vs α

C. Baseline Shuttle Lateral-Directional Controllability Trends

Lateral-directional controllability can be evaluated through comparison of C_L, $dC_n/d\beta$, $dC_l/d\beta$ versus alpha and Mach number. From the above section it is noted that the rolling moment (C_l) and yawing moment (C_n) are both slightly inaccurate.

Turning first to lift, C_L , in FIGURE 21. So long as the wing has a subsonic leading edge, the slope increases with speed; dropping in the supersonics.

FIGURE 22 shows C_l versus C_m. This plot illustrates the increasing stability of the vehicle as Mach increases. We see that for Mach 0.4, the Orbiter is slightly unstable in pitch. At higher Mach numbers, the C_m values become more negative as C_L increases; as the aerodynamic centre shifts aft – the Orbiter becomes stable in pitch.

FIGURE 23 shows how the directional stability strengthens, then weakens as the speed increases. At Mach 2, with a simple vertical fin, the Orbiter becomes slightly unstable directionally.

Similarly, FIGURE 24 shows that the "dihedral effect" seems related to whether the main wing has a subsonic or supersonic leading edge; $dC_l/d\beta$ is somewhat stronger at lower speeds. Overall, the lateral-directional stability of the shuttle is fragile.

During our "calibration" process, reverse engineering the Shuttle Orbiter aerodynamics with panel method codes, we discovered a fascinating phenomenon: that the static lateral-directional stability of the Orbiter depended upon Longitudinal Trim. This effect was not clearly documented in prior literature we were familiar with. We we will discuss this more in a future AIAA conference paper.

V. Computational Study of Variant Shuttle Orbiter Aerodynamics in the Subsonic and Supersonic Flight Regime

A. Dihedral Study

For the various configurations of the shuttle, the designs incorporated the additions of tip verticals. The initial considerations analyzed the effect of the angle of tip dihedral of the tip vertical. This was done in order to determine whether there was an optimal angle for increasing the *LCDP* and $Cn_{\beta DYN}$; see FIGURE 25, overleaf,

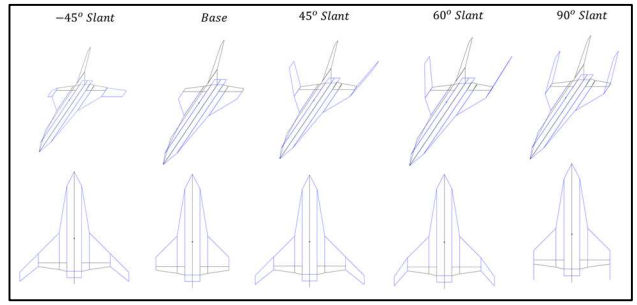

FIGURE 25. Various VORLAX models

The first design of various models that we developed was the tip dihedral of 45°. This design added a tip vertical that extended at a 45° upward tip dihedral, adding an extra 20 feet outboard and 20 feet vertical. Its leading-edge angle maintained the leading-edge sweep of the wing. [38] That being 45° wing sweep leading into the wing tip vertical sweep. The additional wing tip verticals increased the overall wingspan and wing reference area. The changes in wingspan and reference area are shown in TABLE 3.

Model	Sref (ft^2)	Wingspan (ft)
Base	2690	78.1
(-)45 Degree	3160	118
45 Degree	3160	118
60 Degree	3022	106
90 Degree	2690	78.1

For the various other configurations, those being the -45°, 60°, and 90° tip dihedrals, the leading edge sweep and basic areas added for 45° model were maintained throughout. This was done by maintaining the leading-edge length of $20\sqrt{2}$ feet. Again, the leading-edge length was determined by the vertical tip extending an extra 20 feet outward and upward at 45°. The only difference was the tip dihedral angle; refer once again to FIGURE 25.
The impact on $Cn_{\beta DYN}$ can be seen in FIGURE 26. As positive dihedral is added to the outboard panel, the increase in static directional stability and dihedral effect increases $Cn_{\beta DYN}$, a good trend. Conversely, while drooped wing tips increase static directional stability they reduce the effective dihedral of the overall configuration to the point where $Cn_{\beta DYN}$ becomes unstable. The interaction with LCDP is more complex see FIGURE 27.

We see from the Evolved-Bihrle-Weissman Chart (FIGURE 28) that as the angle of the tip dihedral increases, the stability of the vehicle increases; flight exists in Region A. This would indicate that the vehicle goes from a weak departure and spin resistance to a very strong departure and spin resistance. The 90-degree tip dihedral (i.e. vertical tip fins) did best.

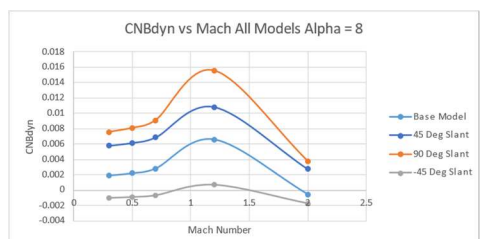

FIGURE 26. $Cn_{\beta DYN}$ *vs* Mach for Different Wing Tip Dihedral

Looking at FIGURES 22, 23 and 24 together we can see that *LCDP* and $Cn_{\beta DYN}$ share a similar trend when compared to the increase in Mach number. They both gradually increase over a small subsonic range, then increase more dramatically and peak around the speed where the wing and vertical leading edges transition from a subsonic to a supersonic leading edge (around Mach 1.25), then begin to precipitously drop off. Above this speed, both trends decline precipitously, indicating the destabilizing nature of increasing Mach number.

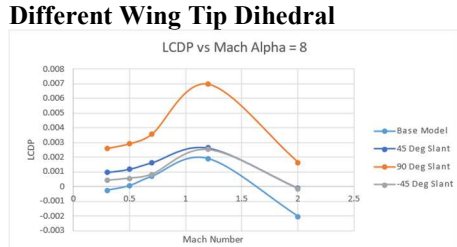

FIGURE 27. LCDP *vs* Mach for Different Wing Tip dihedrals

The impact of angle-of-attack alpha on *LCDP* and $Cn_{\beta DYN}$ for the tip dihedral configurations is seen in FIGUREs 25 and 26. Alpha seems to have a greater impact on $Cn_{\beta DYN}$ than *LCDP*. $Cn_{\beta DYN}$ continues to increase as alpha increases due to the stabilizing effect of sweep at high angles of attack. Conversely, *LCDP* seems to be affected with a shallow drop-off in value as alpha increases at higher Mach values. It contrasts with the lower Mach number cases; these have *LCDP* increasing as alpha increases. This is due to changes in adverse yaw of the aileron as the wing transitions from a subsonic to supersonic leading edge.

Overall, for all the configurations, the 90-degree tip dihedral proved best for the subsonic to supersonic flight regime. For a similar size wing extension, it firmly planted the newly configured shuttle in Region "A" of the Evolved-Bihrle-Weissman. (See FIGURE 28.) The 90-degree tip dihedral further proved that it has the highest values of $LCDP$ and $Cn_{\beta DYN}$ through the various Mach numbers and alphas as seen in FIGUREs 29 and 30. Knowing how $LCDP$ and $Cn_{\beta DYN}$ are influenced by the Mach number and angle-of-attack, that being the overall decrease in effectiveness as Mach number increases would indicate that for the hypersonic flight regime, a configuration that firmly locates the shuttle in Region "A" would be necessary.

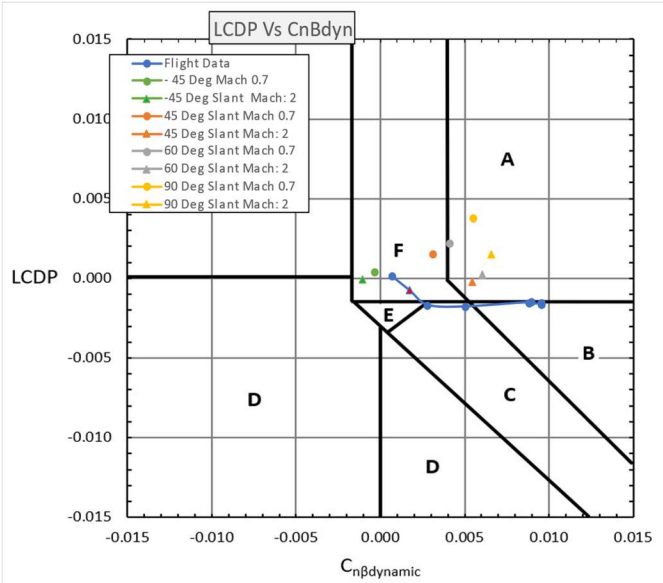

REGION A HIGHLY DEPARTURE AND SPIN RESISTANT
REGION B SPIN RESISTANT, OBJECTIONABLE ROLL REVERSAL CAN INDUCE DEPARTURE AND POST STALL GYRATIONS
REGION C WEAK SPIN TENDENCY AND STRONG ROLL REVERSAL RESULT IN CONTROL INDUCED DEPARTURE
REGION D STRONG DEPARTURE, ROLL REVERSAL, AND SPIN TENDENCIES
REGION E WEAK SPIN TENDENCY, MODERATE SPIN RESISTANCE, AND ROLL REVERSAL, AFFECTED BY SECONDARY FORCES
REGION F WEAK DEPARTURE AND SPIN RESISTANCE, NO ROLL REVERSAL, HEAVILY INFLUENCED BY SECONDARY FACTORS
REGION U HIGH DIRECTIONAL INSTABILITY

FIGURE 28. Evolved Bihrle-Weissman for Various Tip dihedral Configurations.

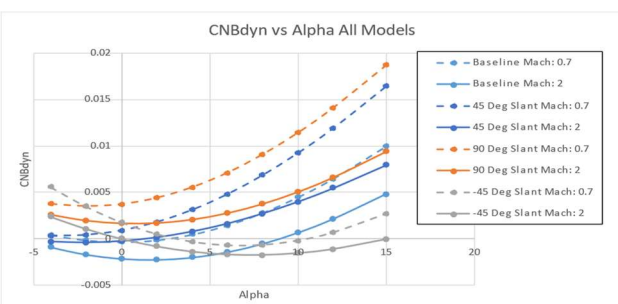

FIGURE 29.$Cn_{\beta DYN}$ vs Alpha

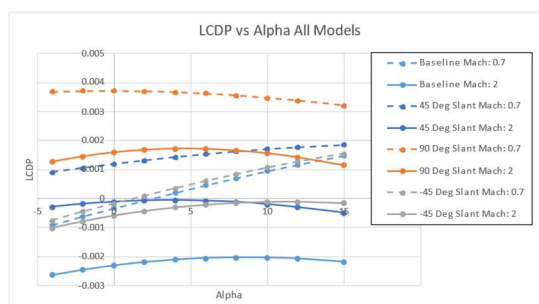

FIGURE 30. LCDP vs Alpha for differing dihedral cases.

B. Wing Tip Sizing Study

At the conclusion of the tip dihedral study, we saw that the 90-degree options proved to be the best option. We conducted a further study to see the impact of the size of tip vertical; see FIGURE 31. The small size had a height of 15 feet, the medium was the 90-tip dihedral height of 28.2 feet and the largest had a height of 35 feet. Because the 90 deg tip dihedral did not extend outward, the wingspan and reference area were the same as the base model.

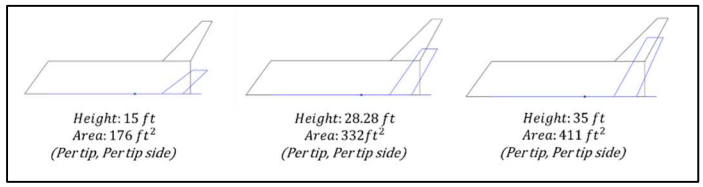

FIGURE 31. Wing Tip Vertical Sizes

When plotting the comparison of the small, medium, and large configurations on the Evolved-Bihrle Weissman, as seen in FIGURE 32, it is clear that the large vertical wing tips did the best at moving the resulting $LCDP$ and $Cn_{\beta DYN}$ values into the "A" Region of the chart. Larger tip fins increase static directional stability, which directly translates to more positive values for both $Cn_{\beta DYN}$ vs. Mach number and $LCDP$ vs. Mach number; see FIGUREs 33 and 34.

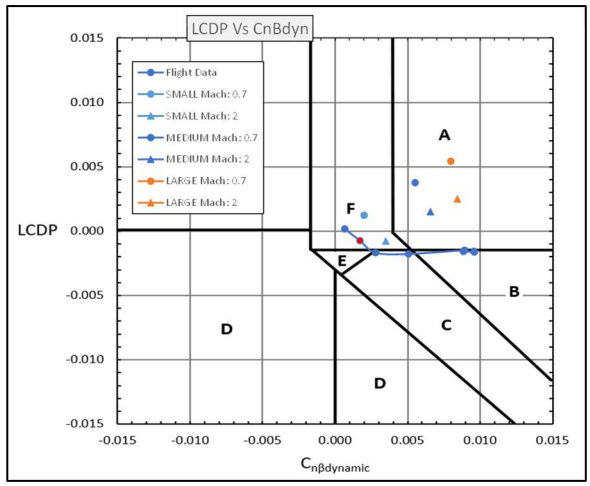

FIGURE 32. Evolved Bihrle-Weissman for Various Wing Tip Fin Sizes

Between our tip dihedral and tip fin size study, we see that fairly large and quite upright tip fins are needed to clean up the aerodynamic controllability at subsonic through supersonic speeds.

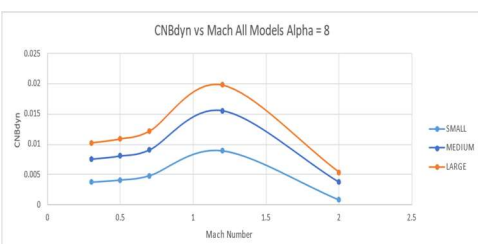

FIGURE 33. Mach vs $Cn_{\beta DYN}$ Different Wing Tip Fin Sizes

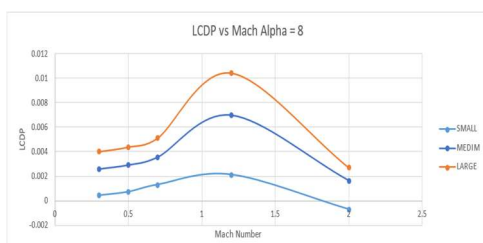

FIGURE 34. Mach vs LCDP for Different Wing Tip Sizes

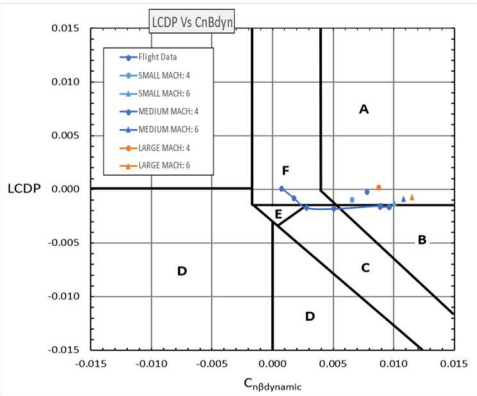

FIGURE 35. Evolved Bihrle Weissman above Mach 2

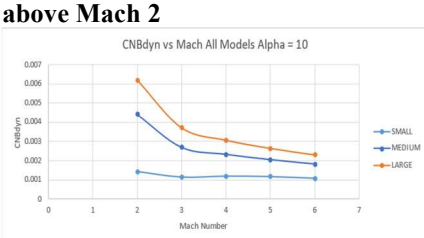

FIGURE 36. Hypersonic Mach vs $Cn_{\beta DYN}$ Different Wing Tip Fin Sizes

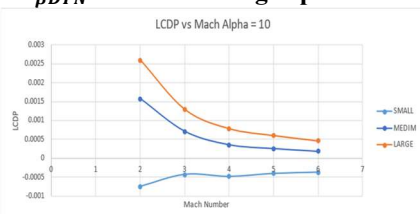

FIGURE 37. Hypersonic Mach vs LCDP for Different Wing Tip Sizes

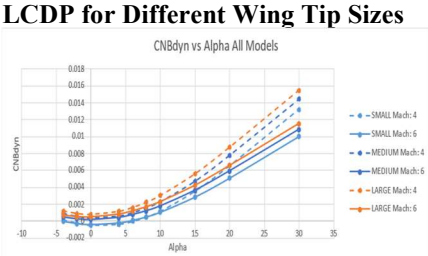

FIGURE 38. Hypersonic $Cn_{\beta DYN}$ vs Alpha for Different Wing Tip Fin Sizes

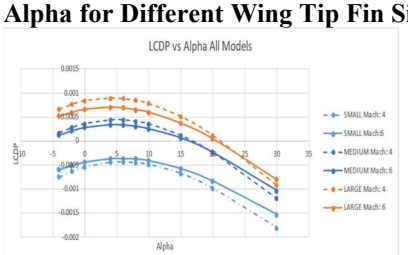

FIGURE 39. Hypersonic Alpha vs LCDP for Different Wing Tip Sizes

V. Computational Study of Variant Shuttle Orbiter Aerodynamics in the Hypersonic Flight Regime

A. Hypersonic Bihrle-Weissman Analysis

The shuttle on reentry had a hypersonic flight regime from Mach 25+ down to Mach 5 and below.

From the tip dihedral study and the wing tip fin size study, the hypersonic study will analyze what we initially considered the "best" configuration for subsonic/supersonic performance. We found that the upright (90º) tip fins performed best and improved the lateral-directional stability. It was further seen that from varying sizes, that the largest vertical tip did best. For the hypersonic portion of the study, it will resume here in comparing the sizes of the tip verticals. For the supersonic/hypersonic analysis, we consider Mach numbers of 2,3,4,5, and 6 over an angle-of-attack (α) range from -4, -2, 0, 4, 6, 8, 10, 15, 20, and 30. Recall that VORLAX's accuracy for lateral-directional stability is "reasonable" up to Mach 5+ when compared to the flight test data.

FIGURE 35 shows the comparison of the wing tip vertical sizes to the Evolved Bihrle-Weissman chart at Mach 4 and Mach 6. While the large tip fins lose some effectiveness as the Mach number increases, they are sufficient to hold still keep the Orbiter in the "A" region.

Similar to the subsonic studies, we see that the *LCDP* and $C_{N\beta dyn}$ versus Mach number holding angle-of-attack constant in FIGUREs 36 and 37. As the speed increases, static directional stability declines leading to a reduction in both terms. FIGUREs 38 and 39 reveal a more fundamental problem, even very large vertical tip fins cannot hold a positive *LCDP* at the highest angles of attack needed to perform the aero-braking maneuver during hypersonic reentry; they help – for sure – but do not eliminate the need for RCS assistance to ensure proper turn-coordination.

Finally, consider FIGURE 40, where we repeat the tip dihedral study but at higher speeds. We can see that all of the cases studied improve controllability at higher Mach numbers.

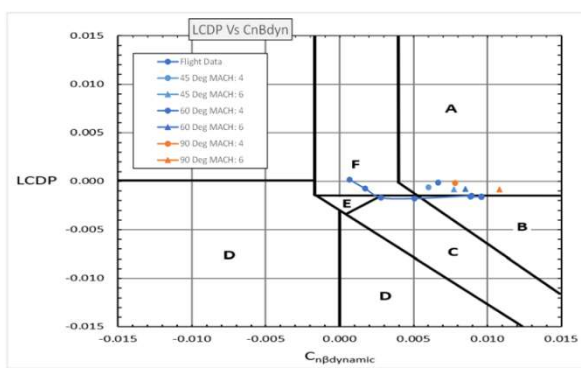

FIGURE 40. Evolved Bihrle-Weissman Wing Tip Dihedral Comparison at Hypersonic Mach Numbers

B. Yaw, Pitch, and Roll Impact

We conclude that the 90º tip vertical of the largest size would be best for improving stability of the vehicle. We demonstrated this in our previous analysis as well as in FIGURE 40 (the Bihrle-Weisman chart). How is yaw, pitch and roll affected?

Using the largest sized 90º Tip from FIGURE 35, for the yaw and roll in FIGURE 41 and 42 respectively, it can be seen that the vehicle is stable throughout. In FIGURE 43, it can be seen that for pitch, the vehicle is unstable at Mach 6. Therefore, a similar, yaw, pitch, and roll analysis was conducted for the 60º tip dihedral from FIGURE 40 at Mach 6 as that is the limiting case.

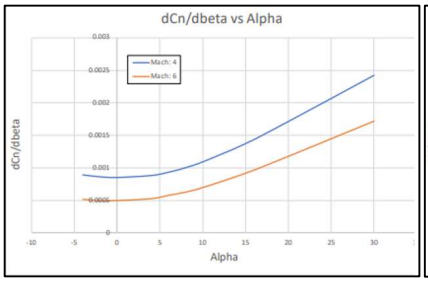

FIGURE 41. Yaw 90-Degree Tips

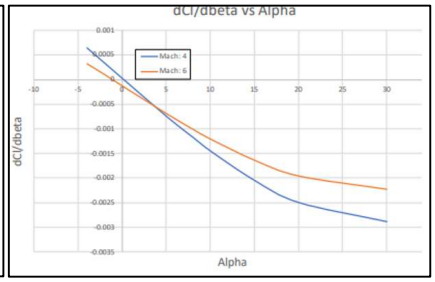

FIGURE 42. Roll 90-Degree Tips

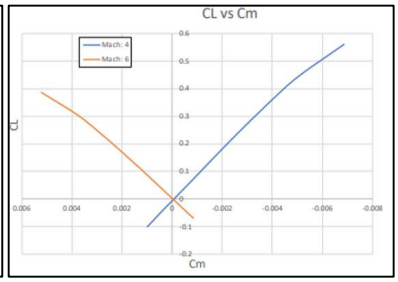

FIGURE 43. Pitch 90-Degree Tips

Here, we see for FIGURES 44 through 46, the vehicle is stable throughout. So, we conclude that the medium sized 60 Degree tip dihedral might be better yet.

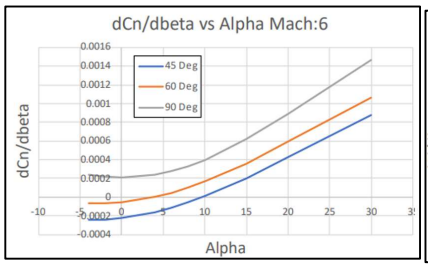

FIGURE 44. Yaw 60-Degree Tips

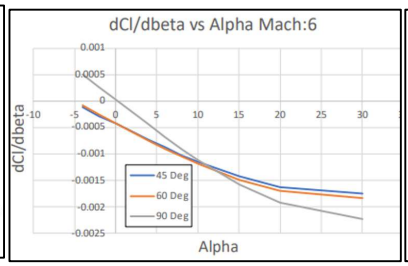

FIGURE 45. Roll 60-Degree Tips

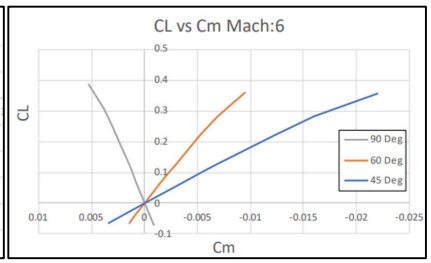

FIGURE 46. Pitch 60-Degree Tips

VI. Assessing Changes to Lateral-Directional Controllability in Light of Longitudinal Stability

In prior sections, we showed how large canted tip fins can improve lateral directional controllability of the shuttle orbiter. However, vehicle design is a multi-disciplinary process – where changes in the aerodynamic configuration are likely to change vehicle mass properties; specifically the longitudinal position of the centre-of-gravity. For all the prior configuration studies of the wing tip treatments, we assumed that the center of gravity would be in the same location as the original Orbiter, 71.40-ft [39] aft of the nose.

The addition of the tip verticals will indeed change the mass moments of inertia for the vehicle as well. This is important due to the impact that the mass moments of inertia have on the $Cn_{\beta DYN}$. Recall equation (1): $Cn_{\beta DYN} = \frac{dCn}{d\beta} * cos(\alpha) - \frac{dCl}{d\,\beta}\left(\frac{I_{zz}}{I_{xx}}\right) * sin(\alpha)$. Note that the mass moment of inertia ratio is a leading coefficient to the rolling moment due to side slip term $(dC_l/d\beta)$. If the desired result in the Bihrle-Weissman chart is to reside in the stable region "A," then $Cn_{\beta DYN}$ must be positive. One way that that is possible is for the rolling moment due to side slip term $(dC_l/d\beta)$ to be negative thus resulting in the addition of the second term. Of course, the angle of attack (α) could cause a sign change, but generally

speaking, if the angle of attack (α) is positive and rolling moment due to side slip term ($dC_l/d\beta$) is negative, then mass moment of inertia ratio could be considered benign due to the addition of two positive values and the sum is greater than +0.004. Therefore, although the CG can move, the moments of inertia are held constant to the original shuttle configuration as long as the resulting rolling moments are negative through the same angles of attack as the yawing moment coefficient is positive. We may verify this with a Bihrle-Weissman analysis.

In this section, we will consider the effects of the 60° dihedral large wing tip extensions in the context of a revised center of gravity (CG) position. We will move the CG both forward and aft of its original location. We varied the XCG location from fuselage stations 65.40, 68.40, 71.40, 72.40, 73.40, 76.40, 79.40, through 82.40-ft; i.e. from 60.6% to 76.3% of the fuselage reference length.

We predict the baseline shuttle to be slightly unstable in pitch at subsonic speeds, 10% stable in pitch at supersonic speeds and neutrally stable in pitch at hypersonic speeds; see FIGURE 47. With the 60° dihedral tip extensions, we can achieve neutral pitch stability at hypersonic speeds with the CG at 73.4-ft (slightly aft of the baseline position); this will make the Orbiter slightly more stable in pitch at supersonic speeds and substantially more stable in pitch at subsonic speeds. In both cases, the aerodynamic centre shifts aft with increasing speed.

Now let us consider the effect of the slightly "aft" of reference CG on lateral-directional stability. If we turn next to FIGUREs 48 and 49, we see that a forward CG broadly increases static directional stability and slightly reduces dihedral effect. A slight aft shift of the CG will not radically disturb lateral-directional stability.

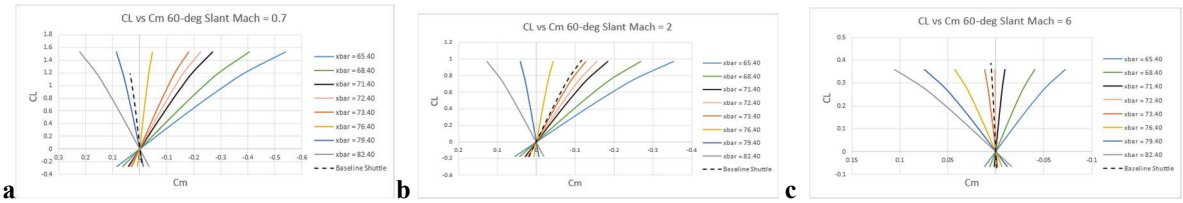

FIGURE 47. Longitudinal Stability (C_L vs C_m) across the flight envelope. a) subsonic, b) supersonic, c) hypersonic

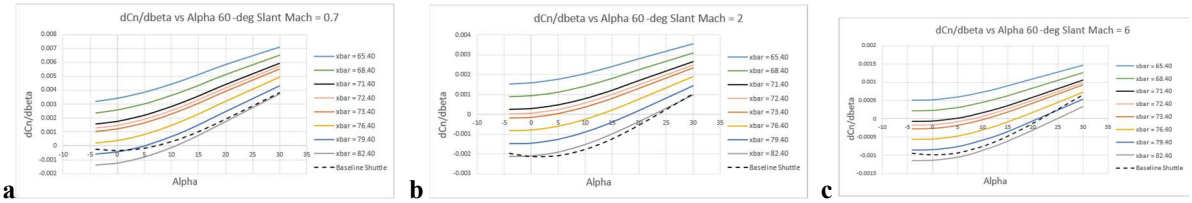

FIGURE 48. Directional Stability ($dC_n/d\beta$ vs α) across the flight envelope. a) subsonic, b) supersonic, c) hypersonic

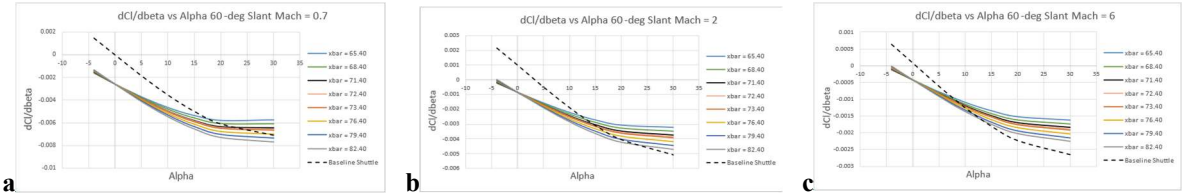

FIGURE 49. Dihedral Effect ($dC_l/d\beta$ vs α) across the flight envelope. a) subsonic, b) supersonic, c) hypersonic

Taken together, the 60° dihedral slanted tip fins appear to be a desirable choice to improve the subsonic, supersonic, and hypersonic stability of the space shuttle Orbiter. They clean up lateral-directional stability, and while they alter longitudinal stability - they do so in a favorable manner – slightly stabilizing rather than destabilizing the airframe. FIGURE 50, overleaf, shows our estimates of un-augmented lateral-directional controllability of the orbiter with the slanted tip fins.

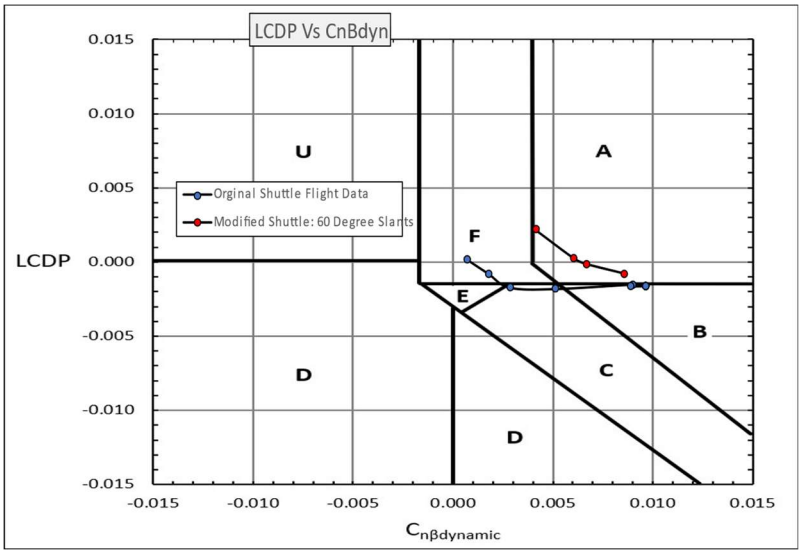

REGION A HIGHLY DEPARTURE AND SPIN RESISTANT
REGION B SPIN RESISTANT, OBJECTIONABLE ROLL REVERSAL CAN INDUCE DEPARTURE AND POST STALL GYRATIONS
REGION C WEAK SPIN TENDENCY AND STRONG ROLL REVERSAL RESULT IN CONTROL INDUCED DEPARTURE
REGION D STRONG DEPARTURE, ROLL REVERSAL, AND SPIN TENDENCIES
REGION E WEAK SPIN TENDENCY, MODERATE SPIN RESISTANCE, AND ROLL REVERSAL, AFFECTED BY SECONDARY FORCES
REGION F WEAK DEPARTURE AND SPIN RESISTANCE, NO ROLL REVERSAL, HEAVILY INFLUENCED BY SECONDARY FACTORS
REGION U HIGH DIRECTIONAL INSTABILITY

FIGURE 50. Evolved Bihrle-Weissman for Final Modified Shuttle with 60-Deg Slanted Wing Tips

VI. Conclusion

This paper shows that the NASA Shuttle Orbiter design had issues with stability that required active control using RCS to compensate for inherent aerodynamic control problems due to the flight regime and its demands. It further shows that because of its multi-regime flight envelope, trade-offs were made to maintain control.

Our first insight is that these problems are not specifically hypersonic issues, as they are seen across the entire flight envelope from subsonic, through supersonic, to hypersonic, and from moderate to high angles of attack. We conclude that a revised configuration with ~60° dihedral tip fins could eliminate a need for RCS jet thrusters for turn-coordination over a fairly large region of the re-entry trajectory. This could free up enough RCS propellant budget to enable substantial increases in hypersonic cross-range and general maneuverability.

Acknowledgements

This manuscript derives from work Mr. Hoopes performed in partial fulfillment of the degree requirements for obtaining his M.S. in Aerospace Engineering from Arizona State University. All design analysis on this unfunded project was completed at Arizona State University. Professor Takahashi would like to thank Professor Ramana Grandhi at the Air Force Institute of Technology for inspiration regarding the subject of this thesis and his generous support of other, parallel collaborative efforts that enabled Mr. Hoopes thesis project.

References

1. *See:* https://www.nasa.gov/centers/dryden/history/pastprojects/HyperX/index.html (accessed Nov. 7, 2022)
2. *See:* https://www.nasa.gov/topics/aeronautics/features/X-51A.html (accessed Nov. 7, 2022)
3. Jenkins, D.R. and Landis, T.R., Hypersonic: The Story of the North American X-15, Specialty Press, North Branch, MN, 2003.
4. Anon., "Proceedings of the X-15 First Flight 30th Anniversary Celebration." NASA CP-3105, 1989.
5. Arrington, J.P. and Jones, J.J., ed., "Shuttle Performance: Lessons Learned," NASA CP 2283 Part 1, 1983.
6. Jenkins, D.R., Space Shuttle: The History of Developing the National Space Transportation System, Walsworth Publishing, Marceline, MO, 1997.
7. Bertin, J.J., Hypersonic Aerothermodynamics, AIAA, 1993.
8. Philips, W.H., "Effect of Steady Rolling on Longitudinal and Directional Stability," NACA TN-1627, 1948.
9. O'Brien, K.P. and Takahashi, T.T., "An Investigation of the Bell X-2 and the Factors that Led to Its Fatal Accident," AIAA 2022-3203, 2022.
10. Takahashi, T.T., "Maneuvering Capabilities of Hypersonic Airframes," AIAA 2023-2247, 2023.
11. Griffin, J.A. and Takahashi, T.T., "Hypersonic Aircraft Performance Limitations Arising from Aerodynamic Control Limits," AIAA 2023-2248, 2023.
12. Griffin, J. A. and Takahashi, T.T., "Aero-Spaceplane Mission Performance Estimations Incorporating Atmospheric Control Limits," AIAA 2022-3656, 2022.
13. Mason, W.H., "High Angle-of-attack Aerodynamics" see: http://www.dept.aoe.vt.edu/~mason/Mason/AeroHighAlpha.html
14. Weissman, R., "Status of Design Criteria for Predicting Departure Characteristics and Spin Susceptibility," AIAA 74-791, 1974.
15. Scheiss, J.R., "Lateral Stability and Control Derivatives Extracted from Space Shuttle Challenger Flight Data," N88-16788, NASA TM 100520, January 1988.
16. Stone, J.S., Baumbach, J.J. and Roberts, B.B., "Space Shuttle Orbiter Reaction Control Subsystem Flight Data Anomalies," NASA CP 2283 Part I, 1983.
17. Cooke, D.R., "Minimum Testing of the Space Shuttle Orbiter", NASA N84 10134, 1983
18. Seltzer, R.M. and Rhodeside, G.R. "Fundamentals and Methods of High-Angle-of-Attack Flying Qualities," Office of Naval Technology AD-A2359 94, January 1988
19. Weissman. R., "Preliminary Criteria for Predicting Departure Characteristics' Spin Susceptibility of Fighter-Type Aircraft," AIAA Journal of Aircraft, Vol. 10, No. 4, April 1973.
20. Takahashi, T.T., Aircraft Performance and Sizing, Volume II: Applied Aerodynamic Design, Momentum Press, New York, 2016.
21. Day, R.E., "Coupling Dynamics in Aircraft Design: A Historical Perspective," NASA SP-532, NASA, 1997.
22. Takahashi, T.T., Griffin, J.A. and Grandhi, R.V., "A Review of High-Speed Aircraft Stability and Control Challenges," AIAA 2023-3231, 2023.
23. Skow, A.M. and Titiriga, A., "A Survey of Analytical and Experimental Techniques to Predict Aircraft Dynamic Characteristics at High Angles of Attack," AGARD CP-235, 1978.
24. Yechout, T.R., Introduction to Aircraft Flight Mechanics, Second Edition, AIAA, 2014.
25. Roskam, J., Airplane Flight Dynamics and Automatic Flight Controls, Pt. I., DAR Corporation, 1995.
26. Roskam, J., Airplane Flight Dynamics and Automatic Flight Controls, Pt. II., DAR Corporation, 1995.
27. MIL-F-8785C, Military Specification: Flying Qualities of Piloted Airplanes, 1980.
28. MIL-STD-1797A, Flying Qualities of Piloted Aircraft, 1995.
29. Compton, H.R., Schiess, J.R., Suit, W.T, Scallion, W.I. and Hudgins, J.W., "Stability and Control Over the Supersonic and Hypersonic Speed Range," NASA CP 2283 Part I, 1983.
30. Kirsten, P.W., Richardson, D.F. and Wilson, C.M., "Predicted and Flight Test Results of the Performance, Stability and Control of the Space Shuttle from Reentry to Landing," NASA CP-2283 Vol. I, 1983.
31. Suit, W.T. and Scheiss, J.R., "Lateral and Longitudinal Stability and Control Parameters for the Space Shuttle Discovery as Determined from Flight Test Data," NASA TM 100555, 1988.
32. Gamble, J., "The Application of Aerodynamic Uncertainties in the Design of the Entry Trajectory and Flight Control System of the Space Shuttle Orbiter," NASA CP 2283 Part 1, 1983.
33. Bourne, C.A. and Kirsten, P.W., "Approach and Landing Characteristics of the Space Shuttle Orbiter," NASA CP 2283 Part I, 1983.

34. Romere, P.O. and Whitnah, A.M., "Space Shuttle Entry Longitudinal Aerodynamic Comparisons of Flights 1-4 With Preflight Predictions," NASA CP 2283 Part 1, 1983.
35. Miranda, L.R., Baker, R.D., and Elliot, W.M., "A Generalized Vortex Lattice Method for Subsonic and Supersonic Flow", NASA CR 2875, 1977.
36. Souders, T.J. and Takahashi, T.T., "VORLAX 2020: Making a Potential Flow Solver Great Again," AIAA 2021-2458, 2021.
37. Gamble, J.D., "The Development and Application of Aerodynamic Uncertainties: and Flight Test Verification for the Space Shuttle Orbiter", NASA - Johnson Space Center Houston, TX, February 21, 1985.
38. Anon., "INVESTIGATION OF THE CHALLENGER ACCIDENT," HR 99-1016, US Government Printing Office, 1986. Vol. 3, Appendix O. See: https://history.nasa.gov/rogersrep/v3o378b.htm
39. Freeman, D.C.,Jr. and Spencer, B.,Jr., "Comparison of Space Shuttle Orbiter Low-Speed Static Stability and Control Derivatives Obtained from Wind-Tunnel and Approach and Landing Flight Tests," NASA Technical Paper 1779, 1980
40. Calloway, R.L., "Lateral-Directional Stability of the Space Shuttle Orbiter at Mach 6," NASA N84-10137,1983